VLHC Design Study Chapter 3

Collider Accelerator Physics and Design

Editors: S. Peggs and M. Syphers
April 13, 2001

DRAFT Version 0.1

Contents

Chapter 3

Collider Accelerator Physics and Design

3.1 TWO COLLIDERS IN ONE TUNNEL

The desire of the feasibility study is to generate a low field (approximately 2 T) collider design in a tunnel which also can be used for a future high field (approximately 10 T) collider. While the second collider is far in the future, one needs to anticipate its requirements as best one can before laying out the components of the first machine since they ultimately must reside in same tunnel. This entails anticipating the geometric requirements, beam optics requirements, and physical space requirements for future technical equipment – much of which may not be known yet.

3.1.1 Footprint Issues

For the design study it has been envisioned that the Low Field (LF) ring will be comprised of long, combined function magnets – the bending of the central trajectory and the focusing of the particle beam will be performed using gradient magnets with a central field strength on the order of 2 T. The High Field (HF) ring will use separated function magnets – dipole magnets for bending the central trajectory and quadrupole magnets for focusing. Since the LF and HF designs have different focusing characteristics, the dispersion suppressors must also be designed simultaneously to ensure that the LF and HF orbits line up appropriately when entering the long straight sections for the Interaction Regions and Utility Regions.

While the size of the arcs is determined primarily by the low magnetic field of the first stage collider, the lengths of the major straight sections are determined primarily by the high magnetic rigidity of the beam in the second stage collider. The interaction regions must be made long enough to accommodate trajectory and optics manipulations of high energy proton beams using reasonable guesses for sizes of future high energy, high luminosity detectors. The utility straight section regions must be made long enough to provide space for extracting a very high energy proton beam toward a beam dump and for beam scraping and beam instrumentation at high energy. All of these functions will be required for the LF collider as well, of course, but the technologies used for injection, extraction, acceleration, and so forth will be similar for the two rings. Thus, the requirements of the HF design will set the scale for the straight sections.

Optics Issues

In addition to the geometric layout of the two rings, many optical properties must be decided simultaneously as well. The Low Field ring uses gradient magnets in the arcs of the collider, while the High Field ring uses quadrupole FODO cells. For simplicity of instrumentation, power distribution, cable runs, etc., it is desirable for the maximum beam size locations in the HF arc to correspond with those in the LF arc. Traditionaly, dispersion suppressor regions are made using “missing magnet” scenarios. The fraction of bending magnets to leave out depends upon the phase advance per cell. In combined function lattices, such as in the LF design, the bending magnets also provide focusing, so this tactic must be modified. While combined function designs of dispersion suppressors have been performed in the past (e.g., Fermilab Recycler), the choice of cell phase advance and cell lengths must be settled upon for both rings to ensure a consistent dispersion suppressor design. (Obviously, this is an issue for both optics and geometry as well.) This is another reason that it was chosen to give the two colliders equal cell lengths and equal betatron phase advances per cell.

Each collider, LF and HF, is made of two separate, but linked, accelerators. The choice must be made as to whether adjacent magnets have the same or opposite focusing characteristic with respect each other for the beam traveling through them. This affects the matching of sections going into and out of straight sections, as well as the design of the beam transfer system joining the LF and HF rings. The decision must be made in coordination with the magnet design effort.

Finally, the magnet choice for the LF collider is a horizontally separated two-in-one iron dominated magnet. To ensure that the two beam trajectories have the same path length, the beams will need to be crossed several times about the circumference. Space and optical designs must be incorporated into the layout to accommodate this feature. The two beams of the high field collider are naturally separated vertically in the common coil arc magnets.

Approach to Design

To allow for lattice and component designs to progress simultaneously for both the LF and HF colliders, a general layout composed of basic modules was developed. As indicated in Figure 3.1, each collider is made up of two major arcs which connect two clusters of straight sections. At the outset, only one cluster region – located at or near the Fermilab site – will be equipped with full IR and UT optics. The other cluster region will have the same straight section lengths, but optically will consist of simpler, FODO-type modules where applicable, with the exception of a special straight section design to accommodate future beam transfers between the LF and HF accelerators.

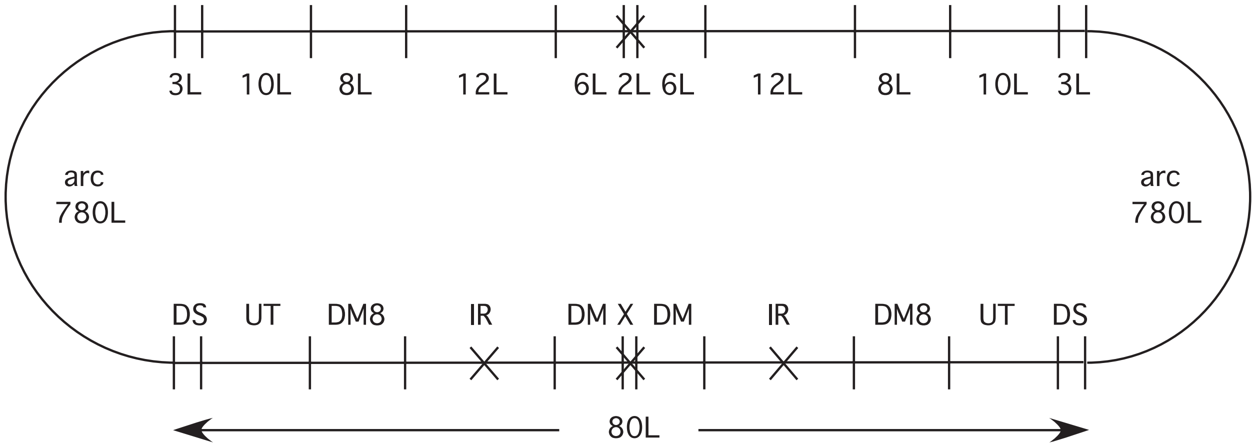

Figure 3.1: Schematic layout of collider modules. The figure is not to scale, emphasizing the straight section functions.

By scaling the Tevatron half cell length to the LF energy, the distance between quadrupoles in the arcs of the new colliders would be approximately 135 m. The HF ring could probably tolerate longer cells, but stronger focusing will be adopted to be consistent with the LF ring. The exact length of the standard cell will be determined by the chosen bunch spacing. To ensure that bunches will collide at any detector in the design, regardless of what modules exist between interaction points, the ring module lengths are designed in units of the bunch spacing.

Dispersion suppressor modules are adopted following the SSC design, which was also later used in the Fermilab Main Injector. A cell phase advance of 90 degrees has been chosen for which a dispersion suppressor can be made using four special cells, each 3/4 the length of a standard cell and each containing 2/3 the bending of a standard cell. These modules reduce the periodic arc dispersion function to zero at the output of four such cells. The short bending regions between Interaction Regions and Utility Regions will be composed of back-to-back dispersion suppressor modules. If additional bending is required in these regions, it can be generated by inserting standard half cells between the DS modules.

3.1.2 Footprint and optical modules

Table 3.1 lists the fundamental parameters of the footprint. In the transition from Stage 1 to Stage 2 operation, the experiments will remain centered on the same interaction points. At the same time it is envisaged that they will be upgraded to take up more space along the beam line, increasing the distance from the IP to the first magnet, L^*, from 20 to 30 m. It is therefore necessary to allow for a bypass to keep the low field ring beams well clear of the experiments . This must be done without changing the total low field ring circumference.

One advantage of modular construction is that low and high field lattices are guaranteed to have almost identical footprints, and therefore to fit in the same tunnel, so long as corresponding low and high field modules are placed on top of each other. The maximum deviation is only a few millimeters, easily allowing one ring to be placed on top of the other at all locations in the VLHC tunnel.

Circumference, C	233.037	km
Average arc radius, R	35.0	km
Number of interaction points	2	
Half cell length, L_{hc}	135.486	m
Half cell bend angle, θ_{hc}	3.875	mrad
Half cell count	1720	
Half cell harmonic, n_λ	24	
Bunch spacing (53.1 MHz), S_B	5.645	m
	18.8	ns
Number of buckets	41280	
Number of bunches, M	37152	
Phase advance per cell	90.0	deg
Revolution frequency	1.286	kHz
Revolution period, T	.778	ms
Harmonic number, h	371520	
RF frequency (9 × 53.1)	478.0	MHz

Table 3.1: Fundamental lattice parameters common to both low and high field rings.

Half cell length

The average bending radius of the arcs is made as close as possible to the goal value of $R = 35$ km by adjusting the total equivalent number of (bending) arc cells in each ring. Each of the 4 short half cells in each dispersion suppressor has 2/3 the bending of an arc half cell. Thus, the 20 dispersion suppressors (on either side of 10 straights) have a total bending equivalent to 160/3 arc half cells. If there are $N = 784$ arc half cells in each half of the VLHC, then the bend per half cell is

$$\theta_{hc} = \frac{2\pi}{2N + 160/3} = 3.875 \ \ [\mathrm{mrad}] \tag{3.1}$$

and the average arc bend radius is

$$R = \frac{L_{hc}}{\theta_{hc}} = 34.961 \ \ [\mathrm{km}] \tag{3.2}$$

The (minimum) bunch spacing S_B is taken to be one 53.1 MHz RF wavelength in the Tevatron

$$S_B = \lambda_{53} \equiv \frac{2,000\pi}{1113} = 5.645 \,\mathrm{meters} \tag{3.3}$$

This guarantees that the filling schemes from the Tevatron will be relatively simple. The bunch time spacing of about 18.8 ns is not unreasonably challenging to the experiments.

The half cell length is

$$L_{hc} = n_\lambda S_B \tag{3.4}$$

The bunch spacing can trivially be increased (for example during commissioning) by any of the common factors of the "half cell harmonic number" n_λ. The value of $n_\lambda = 24$ was chosen for both low and high field rings in the VLHC Feasibility Study [1], corresponding to a half cell length of $L_{hc} = 135.4865$ meters.

This half cell length is short enough to keep the natural horizontal emittance due to synchrotron radiation in the high field ring, $\epsilon_{nat} = 0.04$ μm, much smaller than the horizontal emittance $\epsilon_x \approx 0.20$ μm which must be maintained (by heating) to avoid beam-beam limits in the store. A stronger limit to the maximum arc half cell length is the need to limit the vulnerability of the low and high field rings to systematic field harmonic errors in the arc bending magnets. This is more critical for the low field ring, simply because the injection energy is an order of magnitude lower (1 TeV) than for the high field ring (10 TeV).

The current value of $L_{hc} = 135.4865$ m is by no means fully optimized, not least because we do not accurately understand what values of systematic magnet harmonics might be achieved in industrial production of the arc bending magnets.

3.2 STAGE 1: THE LOW-FIELD RING

The first stage low-field collider will have a top energy of 20 TeV and peak (initial) luminosity of 10^{34} cm^{-2}sec^{-1}. The collider will use the Tevatron as its injector operating at a transfer energy of 900 GeV. For this study a transverse emittance of 1.5π mm mrad (rms, normalized) is used, which is typical for the Fermilab Booster, though about half the value at the Tevatron under recent normal operations. It is anticipated that with further Run II experience, the efficiency of emittance preservation will increase. Using the present acceleration systems of the Tevatron injector chain, the collider has a bunch spacing of 5.645 m (53.1 MHz) which sets the number of available RF buckets. With a 90% filling fraction to allow for gaps in the beam for various kicker rise times, the number of protons per bunch required in the Stage 1 collider is approximately 2.6×10^{10}, similar to Tevatron bunch intensities during previous Fixed Target operations. Using an interaction region design with a $\beta^* = 0.3$ m, we arrive at the desired initial luminosity. Table 3.2 lists the general parameters of the Stage 1 collider.

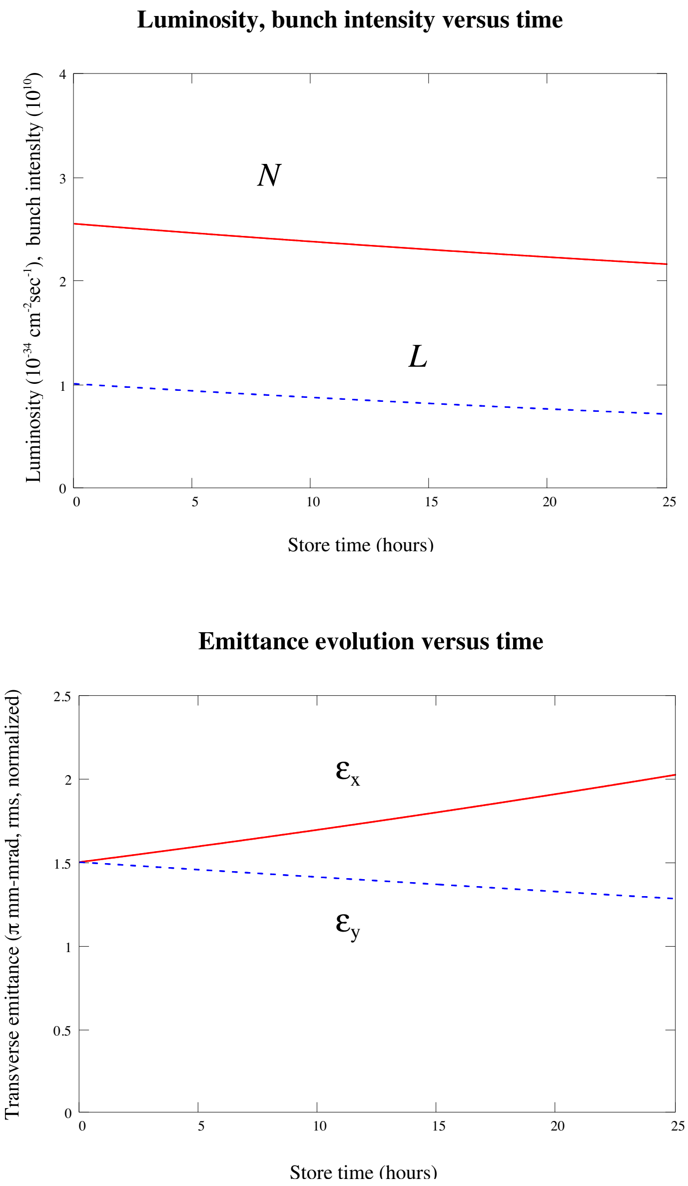

Figure 3.2: Evolution of collider parameters during a typical store.

Typical store parameter evolution is depicted in Figure 3.2. The figure shows the proton bunch intensity and luminosity decreasing due to collisions. The vertical emittance also decreases slightly due to synchrotron radiation damping which occurs with a damping time of about 100 hr. Due to the use of gradient magnets in the Stage 1 collider the horizontal emittance actually will be *anti-damped*, and will increase at approximately the same rate. This should not be a problem since store times will be much less than 100 hours.

Storage energy	20	TeV
Peak luminosity	10^{34}	$\mathrm{cm}^{-2}\mathrm{s}^{-1}$
Packing fraction	89	%
Injection energy	0.9	TeV
Transverse normalized emittance, rms (H&V, inject)	1.5	μm
Initial bunch intensity	2.6×10^{10}	
Average beam current	195	mA
Stored energy per beam at collision	3.0	GJ
Bend field at storage	2.0	T
Bend magnet gradient	9.0	T/m
Phase advance per cell	90.0	deg
Max RMS arc beam size (inject)	1.2	mm
Bunch spacing (53.1 MHz)	5.645	m
	18.8	nsec
Bunch length	30	mm
Longitudinal emittance, rms (inject)	0.4	eV-s
RF voltage at storage	50	MV
Fill time	60	min
Acceleration time	1000	sec
Beam size (rms) at IP (storage)	4.6	μm
Total crossing angle (10σ separation in drift space)	153	μrad
Distance from IP to first magnet	21	m
β^* at IP (H & V)	0.3	m
Maximum interactions per crossing	20	
Debris power at IP (each direction)	3	kW
SYNCHCROTRON RADIATION AT STORE		
Energy loss per turn per particle	38	keV
Radiation damping time (τ_0)	100	hr
(anti-damping in H plane)		

Table 3.2: Nominal stores parameters for the low field collider.

3.2.1 Lattice

The bulk of the lattice is characterized by its construction from just three optical building blocks - arc, dispersion suppressing, and straight-section cells. The arc and suppressor cells have space allocated at maximum-β sites for 4 correction elements. Additional corrector space is available at the quarter-cell locations ($\beta_x = \beta_y$) for lumped correction of systematic multipoles.[31]

Two utility straights, each of which must accommodate 900 GeV injection from the Tevatron plus abort of 20 TeV beams are shown. The beams collide with a horizontal crossing angle at two interaction points where β_{max} = 30 cm. In a special cell, midway between the IP's, the beams are made to cross over between the inner and outer horizontal apertures. Diametrically opposed in the ring, a mirror of this cell is installed to ensure identical path lengths for the two circulating beams.

Interaction Regions

The final foci in the IR's are anti-symmetric triplets, formed from single-bore, 300 T/m magnets. Four additional quadrupole circuits, comprising double-bore, 70 T/m magnets, are also used in optical matching. With a total of 6 independently-tunable quadrupole circuits available it is possible to match the four β's and α's from the IP to regular FODO cells, and hold the phase advance $\Delta\mu$ constant across the IR through the squeeze from β^* = 6.00 m $\rightarrow$ 0.30 m. Fixing $\Delta\mu$ eliminates the necessity of a special phase trombone to maintain the nominal operating point. Figure 3.3 shows the lattice functions through the IR during collisions.

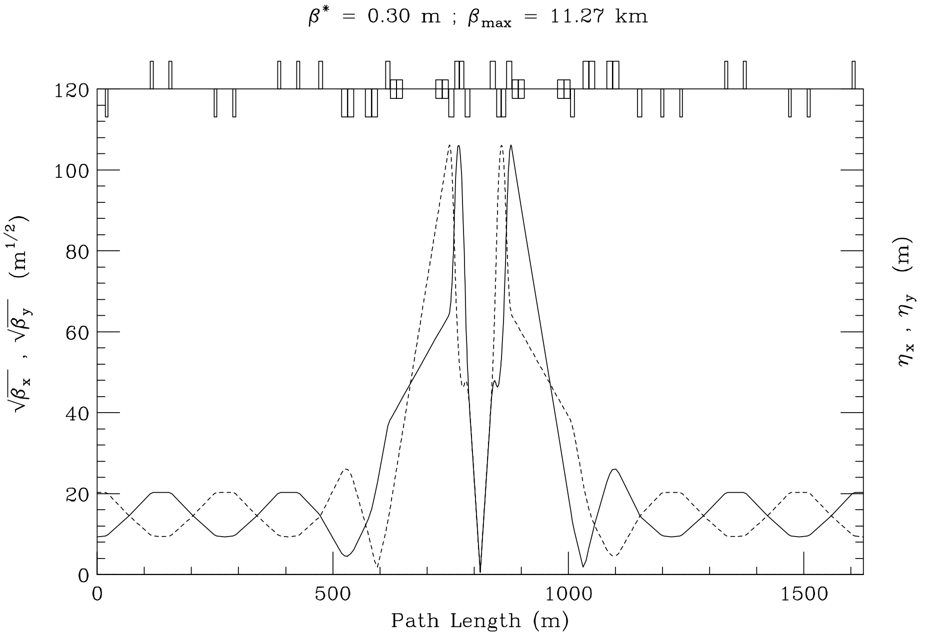

Figure 3.3: IR lattice functions in the collision configuration.

The circulating beams are separated horizontally by 15 cm throughout the arcs and 70 T/m straight-section quads. Four dipoles, 13.6 m each at 1.97 T, situated between the Q3 and Q4 quadrupoles bring the beams together at the entrance to the triplet for collisions at the IP. Dipoles downstream of the IP separate the beams again and channel them back into the inner and outer rings. A half-crossing angle of 77 μr at the IP gives 10σ separation between the beams at the first parasitic crossing.

Injection and Abort Straight Sections

To accommodate 900 GeV injection from the Tevatron, as well as 20 TeV proton abort, 5 straight-section cells are modified as shown in Figure 3.4. A long drift space (377 m) is created by triplet focusing to produce sufficient room for abort Lambertsons (not shown) and beam extraction.

Dipoles separate the circulating beams through the utility straight to make room for RF cavities downstream of the second triplet. Three 21.54 m dipoles at 2 T bend the beams apart by 40 cm, followed immediately by 3 more dipoles that flatten out the trajectories. This pattern is reversed downstream of the RF to bring the beams back into standard double-bore magnets.

Beam Crossovers

With the beams separated horizontally in the arcs it is necessary to move the beams between the inner and outer rings to maintain identical path lengths. In the LF ring 2 cross-over cells are inserted on opposite sides of the ring. Four rolled dipoles move the beams the 15 cm from one channel to the other. Each dipole is 36 m at 1.944 T. The first dipole is rolled by0.12 rad to start separating the beams vertically, while bringing them closer together horizontally. The second bend is rolled by -0.12 rad to flatten the vertical trajectory. At the crossing point the beams are separated vertically by 9 mm. This is 17.8σ

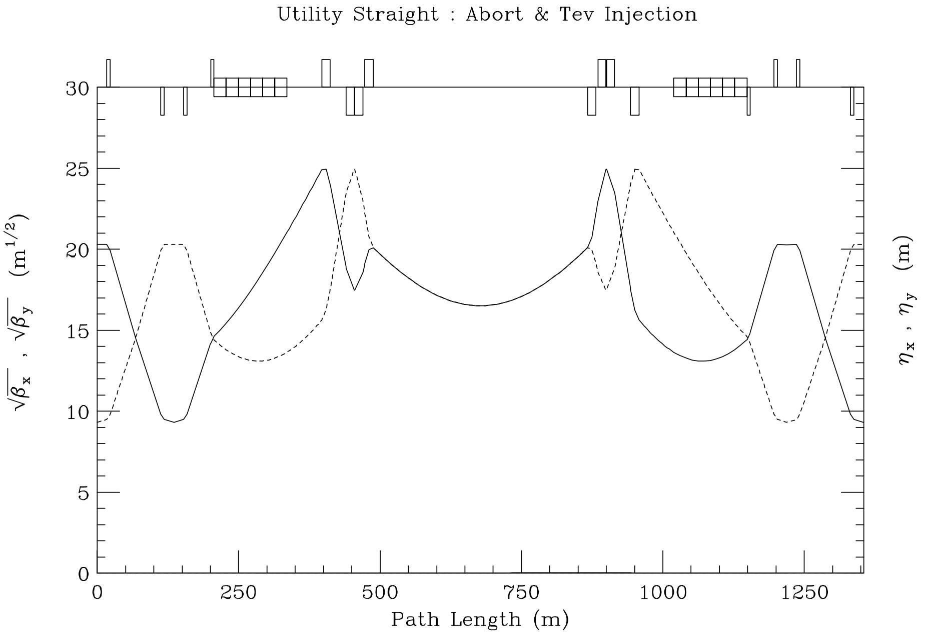

Figure 3.4: Layout of a utility straight supporting beam transfer from the Tevatron and 20 TeV abort.

at the injection energy of 900 GeV. Rolled dipoles after the crossing point remove the vertical offsets and complete the 15 cm transverse transfer of beams to the opposite channel.

Miscellaneous Insertions

For momentum collimation a localized dispersion wave is generated in a 5-cell straight section (Figure 3.5). Four 45 m dipoles (2T @ 20 TeV) at the upstream end of the straight move the beams transversely by 0.36 m, creating $\pm$70 cm of dispersion. Four more dipoles downstream bring the beams back onto their nominal trajectory and cancel the dispersion.

Free space can be created in the arcs by replacing standard arc gradient magnets with a shorter, modified version plus a small quadrupole. Through this insertion, the β's, α's, and phase advance of an arc cell are exactly reproduced by a gradient magnet with B' = 9.185 T/m (1% weaker than the regular arc magnets) plus a 2.0 m quadrupole with B' = 26.14 T/m. The low field of the quadrupole makes it just a longer version of the normal arc trim quads. The dispersion wave created by the holes is cancelled locally with 90° of phase advance per cell.

3.2.2 Magnet apertures and Field Quality

The required dynamic aperture is determined by the available mechanical aperture. Collimators define the limiting aperture in most cases and they are usually placed at around 6σ from the center of the beam pipe. This allows 3σ for the beam distribution, and another 3σ for injection errors and orbit drifts over time. The real dynamic aperture therefore must be greater than 6σ in order to avoid significant losses of particles at places in the ring outside the beam cleaning section.

Errors, time dependent fields and other imperfections in a real machine can never be modelled accurately enough in a simulation so the dynamic aperture calculated by a simulation always exceeds the measured dynamic aperture. Observations at the Tevatron, HERA, and SPS have shown that the agreement between the measured and calculated dynamic aperture varies between 20-100%. As a consequence the LHC, for example, requires that the calculated dynamic aperture after 10^5 turns at both injection and collision (with only magnetic nonlinearities) equal 12σ. Since the errors listed above are just as likely for the VLHC, it seems reasonable to adopt a dynamic aperture requirement of 12σ after 10^5 turns.

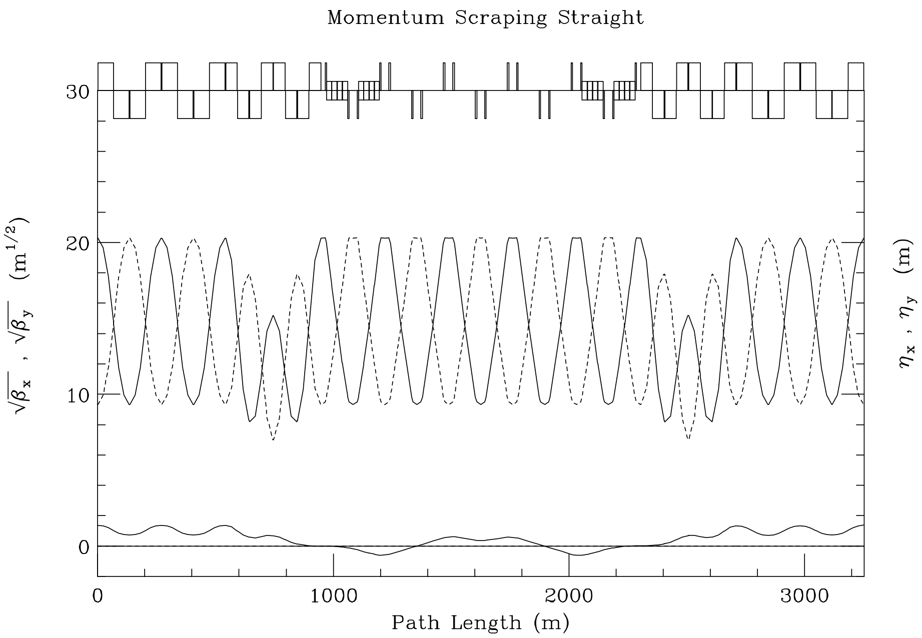

Figure 3.5: Dispersion creation in a 5-cell straight for collimation.

Scaling the Main Injector errors

The field harmonics in the low-field magnets will be measured in the summer or fall of 2001. As a starting hypothesis, the errors in the Main Injector are used as a scaling basis, assuming that the mechanical errors scale with the pole tip gap. Thus we assume that the field errors in the VLHC low field transmission line magnets at a pole tip radius of 10 mm are the same as the errors in the Main Injector magnets at a pole tip radius of 1 inch. The bend fields in the Main Injector at 8 GeV and in the VLHC at an injection energy of 1 TeV are nearly the same: B_0^{MI}= 0.101 T, B_0^{VLHC}= 0.098 T.

We make the somewhat stronger assumption that the equality is satisfied for every harmonic n so that we obtain the following scaling relation between the multipole coefficients in the Main Injector and those in the VLHC,

$$\left[\frac{b_n}{R_{ref}^n}, \frac{a_n}{R_{ref}^n}\right]^{VLHC} = (2.54)^n \times \left[\frac{b_n}{R_{ref}^n}, \frac{a_n}{R_{ref}^n}\right]^{MI} \quad (3.5)$$

Order n	$\langle b_n \rangle$	$\langle a_n \rangle$	$\sigma(b_n)$	$\sigma(a_n)$
2	-0.600	0.000	0.600	0.200
3	0.000	0.00	0.149	0.300
4	0.300	0.000	0.300	0.150
5	0.000	0.000	0.100	0.500
6	0.000	0.000	0.250	0.250

Table 3.3: Systematic $\langle\rangle$ and random σ of multipole coefficients used for the VLHC, scaled from Main Injector magnets using Equation (3.5). The coefficients are shown in units of 10^{-4}, at a reference radius of 10 mm.

Table 3.3 shows the derived harmonics for the low field magnets. We have assumed that the measured systematic skew harmonics in the Main Injector magnets are the result of the top down asymmetry in the magnet bus work [32]. This should not be an issue for the low-field magnets since the bus work is symmetric, and so the nonlinear skew harmonics have been set to zero.

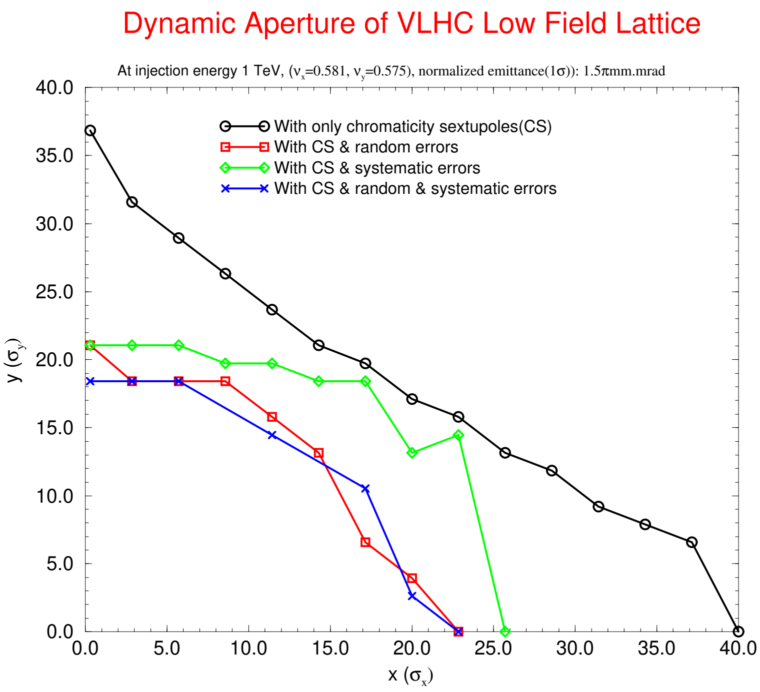

Figure 3.6: Dynamic aperture at injection with only chromaticity sextupoles, only random errors, only systematic and all errors.

Dynamic aperture at injection

The main issue is to determine whether the field quality is good enough to meet the target set for the acceptable dynamic aperture. If not, a nonlinear corrector system that increases the dynamic aperture to the target value must be developed. The results shown below will be refined at a later stage when more information on the field quality is available. For most calculations reported here, particles are tracked for 1024 turns without synchrotron oscillations in a perfectly aligned lattice. The only nonlinearities are the chromaticity sextupoles and the field errors in the arc magnets. Sources of coupling are not introduced so correction with skew quadrupoles is not necessary. The fractional tunes are set to the Tevatron values ν_x =0.581, ν_y = 0.575.

Figure 3.6 shows the dynamic aperture with only chromaticity sextupoles, only random errors, only systematic errors and all the errors. The dynamic aperture with all errors is nearly the same as that with only the random errors. Tracking with all the field errors at injection shows that the dynamic aperture is about 20σ as shown in Table 3.4. Increasing the number of turns to 100,000 typically results in a decrease of the dynamic aperture by about 2-3σ. This suggests that the target dynamic aperture of 12σ at 100,000 turns should be met with this set of assumed errors.

The impact of linear coupling is reduced when there is a difference in horizontal and vertical integer tunes. In the perfect aligned lattice there are no sources of linear coupling. Nevertheless we studied the influence of tune splits on the dynamic aperture for the cases $\nu_x - \nu_y = \pm 2, \pm 4, \pm 6$. In no case did the dynamic aperture improve and in some cases the aperture was reduced significantly, presumably due to the beta beating.

Dynamic aperture at collision

The dynamic aperture at collision optics will be dominated by the field errors of the IR quadrupoles due to the large beam sizes in these magnets. The IR quadrupoles with their high gradients will be built with “conventional” superconducting magnets. The nonlinear harmonics in these magnets are well understood following decades of development and also through the Fermilab program of building these quadrupoles for the LHC. The errors in the arc magnets built with conventional technology usually are not significant in determining the dynamic aperture at top energy. For example, the target dynamic aperture in the LHC at

Errors	Dynamic Aperture (σ)	
	Average	Minimum
Only chromaticity sextupoles (CS)	30.9	25.4
CS and only random errors	20.0	18.4
CS and only systematic errors	23.4	21.1
CS and all errors	19.7	18.4
CS and only random errors and $\sigma(b_2) = \sigma(a_2) = 0$	20.4	18.6
CS and only random errors and $\sigma(b_3) = \sigma(a_3) = 0$	20.2	17.6
CS and only $\langle b_2 \rangle \neq 0$	31.5	25.2
CS and only $\langle b_4 \rangle \neq 0$	24.5	21.1

Table 3.4: Dynamic aperture at injection energy with various sets of errors in the arc magnets. These results show that the random errors together have a somewhat larger impact on the dynamic aperture than the two systematic components $\langle b_2 \rangle$, $\langle b_4 \rangle$. The dynamic aperture with all the errors is about the same (20σ) as without the systematic errors.

top energy is set at 12σ with only the IR quadrupole field errors. We will adopt the same target dynamic aperture of 12σ in the simulations.

The arc magnets in the Stage 1 collider, however, are built with transmission line magnets which have different characteristics from conventional superconducting magnets. At high current, the field in the iron saturates leading to a drop in the gradient and a large negative sextupole component (b_2). While the change in gradient will be compensated by quadrupole correctors in every cell to maintain the correct phase advance per cell, the compensation of the sextupole component is a more serious issue. If the nonlinear fields due to magnet saturation have a significant impact on the dynamic aperture, then this could potentially limit the maximum energy reach of the low field collider.

The straightforward approach to compensating the saturation b_2 component is to use the chromaticity sextupoles in the cells to correct the linear chromaticity. At large $|b_2|$ this leads to strong chromaticity sextupoles lumped at two locations in the cell, one SF next to the focusing magnet (F), the other SD next to the defocusing magnet (D). A calculation of the dynamic aperture at 20 TeV without the IR errors but with the b_2 component in the arc magnets due to saturation shows that the dynamic aperture is quite large even up to 10 units of b_2. At $b_2 = 0$, integrated strengths required for the F and D type sextupoles are (946, 1761) T/m respectively. At positive $b_2 \leq 3$, the F sextupoles decrease and D sextupoles increase in magnitude and vice versa at negative $b_2 \geq -3$. At larger absolute values of b_2, both sextupoles increase in magnitude. If required, additional sextupoles could be placed in the 1 m gap between the F and D and the D and F magnets to correct the chromaticity generated by the iron saturation. This would lower the integrated sextupole strengths and allow for larger values of b_2 to be compensated.

The impact of magnet saturation should, however, be determined in the presence of the dominant field errors of the IR quadrupoles. We have based our dynamic aperture calculations on the expected field errors calculated by G. Ambrosio et al. [35].

The dynamic aperture was calculated for three seeds for the random errors with the signs of the uncertainties in the systematics alternating between positive and negative. The random errors were truncated at 3σ. For each seed the dynamic aperture was calculated with $-10 \leq b_2 \leq 10$. At $b_2 = 0$, the dynamic aperture drops to around 20σ in the presence of the IR errors, compared to a value of around 130σ without these errors but only chromaticity sextupoles. The average dynamic aperture varies over a small range of 20-23 σ when $|b_2| \leq 10$. Clearly the saturation sextupoles do not have a significant impact on the dynamic aperture at 20 TeV. The maximum tolerable value of b_2 may instead be limited by the sextupole strengths required to correct the chromaticity.

Some limited tracking results with synchrotron oscillations (period about 500 turns) for 10,000 turns and $\delta p/p = 3 \times 10^{-4}$ show that the dynamic aperture is nearly the same over the range of $-10 \leq b_2 \leq 10$. These preliminary results indicate that this range of variation in b_2 does not significantly limit the momentum aperture.

3.2.3 Tolerances and Corrections

Closed orbit

Distortions of the ideal closed trajectory in the collider will be primarily generated by transverse alignment errors. The trajectory in the horizontal plane will also be influenced by errors in the main bend field of the magnets, and the vertical trajectory will be further distorted due to roll errors in the main bending field.

For a bending magnet of length L with gradient B' which is displaced transversely from its ideal position by an amount d, a particle with magnetic rigidity $B\rho = p/e$ will have its trajectory deflected through an angle $\theta = (B'L/B\rho)\cdot d$. For the low field collider, the gradient magnets have lengths roughly equal to the half-cell length and will be supported along its length by several adjustable magnet stands. If the arc magnets are divided into n equal-length sections for support and alignment, then the rms expected closed orbit deviations in the horizontal (x) and vertical (y) degrees of freedom at maximum β locations in the arcs are given by

$$\Delta\hat{x}_{co} = \frac{\sqrt{\hat{\beta}\langle\beta\rangle}}{2|\sin\pi\nu|}\sqrt{\frac{N}{2}}\left(\frac{B_0L}{B\rho}\right)\sqrt{\frac{1}{n}\left(\frac{B'd_{rms}}{B_0}\right)^2 + \left(\frac{\Delta B}{B_0}\right)^2_{rms}}$$

and

$$\Delta\hat{y}_{co} = \frac{\sqrt{\hat{\beta}\langle\beta\rangle}}{2|\sin\pi\nu|}\sqrt{\frac{N}{2}}\left(\frac{B_0L}{B\rho}\right)\sqrt{\frac{1}{n}\left[\left(\frac{B'd_{rms}}{B_0}\right)^2 + \phi^2_{rms}\right]}$$

where $(\Delta B/B_0)_{rms}$ is the rms field strength deviation of the full magnet, d_{rms} is the rms displacement at the n locations, and ϕ_{rms} is the rms roll angle (with respect to vertical) at the n locations within a half-cell. N is the number of half-cells in the collider.

For typical values of the above variables we use n = 5 over a half cell length of L = 67 m, $\hat{\beta}$ = 411 m, $\langle\beta\rangle$ = 250 m, B_0 = 2 T, B' = 9 T/m, d_{rms} = 250 μm, ϕ_{rms} = 0.5 mrad, and $(\Delta B/B_0) = 10^{-4}$. From a distribution of errors over the 780 arc cells in the collider, we obtain expected rms orbit errors on the scale of

$$\Delta\hat{x}_{co} \approx 9.5\,\mathrm{mm},$$

$$\Delta\hat{y}_{co} \approx 10.3\,\mathrm{mm}.$$

The uncorrected closed orbit clearly ventures outside any reasonable beam pipe radius.

To correct the orbit distortions, we assume dipole correctors are placed at maximum β locations in the arcs, and a standard 3-bump algorithm is performed. The corrector strength necessary to perform the correction using the parameters introduced above would be

$$\Theta_x = \frac{\sqrt{2}}{\sin\mu}\sqrt{\frac{\langle\beta\rangle}{\hat{\beta}}}\left(\frac{B_0L}{B\rho}\right)\sqrt{\frac{1}{n}\left(\frac{B'd_{rms}}{B_0}\right)^2 + \left(\frac{\Delta B}{B_0}\right)^2_{rms}}$$

and

$$\Theta_y = \frac{\sqrt{2}}{\sin\mu}\sqrt{\frac{\langle\beta\rangle}{\hat{\beta}}}\left(\frac{B_0L}{B\rho}\right)\sqrt{\frac{1}{n}\left[\left(\frac{B'd_{rms}}{B_0}\right)^2 + \phi^2_{rms}\right]}$$

where μ is the cell phase advance. For μ = 90°, and the same parameter values as before, the rms corrector strengths are

$$\Theta_x \approx 2.3\,\mu\mathrm{rad},$$

$$\Theta_y \approx 3.2\,\mu\mathrm{rad}.$$

At 20 TeV, a 3 μrad bend angle requires an integrated field strength of 0.2 T-m. To be able to correct at the 2.5-σ level, the steering correctors should have strengths of approximately 0.5 T-m.

Quadrupole effects

The quadrupole gradient in the transmission line magnets drops steeply at high fields due to saturation of the iron. Quadrupole correctors, one in each plane, will be placed in every arc cell to maintain the required phase advance of 90° per cell. At present these correctors are 0.5 m long and placed at the beginning of each half cell. A 5% drop in the gradient of the main magnets at 2.0 TeV will require a gradient of 80 T/m in these correctors to maintain the phase advance in the cells.

Sources of errors in the tune include gradient errors and closed orbit distortions in the nonlinear magnets. Quadrupole correctors in the arcs will be used to control the global tunes and to split the integer tunes to reduce the sensitivity to systematic linear coupling sources.

It will be important to restrict the beta-beating to a low value everywhere, both for on-momentum and off-momentum particles. It will be specially important to isolate the interaction regions from beta-beating errors generated elsewhere in the ring. Quadrupoles at the entrances and exits of the arcs and at the entrances and exits of the straight sections can be used to control both the amplitude and phase of $\Delta\beta/\beta$.

Normal quadrupole gradient errors and skew quadrupole gradient errors will contribute to horizontal and vertical dispersion beating respectively. The errors generated in the arcs and utility straight sections will be corrected either by quadrupole correctors or by the closed orbit correctors. It will be important to keep the dispersion at the IPs very small. Local dispersion correction within the IRs will be necessary to correct the dispersion generated by the crossing angle.

Coupling

Sources of coupling include skew quadrupole errors in the main magnets, rolls of the gradient magnets and vertical orbit distortion through the nonlinear magnets. The tolerance for the allowed coupling may be set by requiring that the minimum tune split be less than 0.05 before correction. Larger values make coupling correction with skew quadrupoles difficult.

Skew quadrupoles placed in regions of horizontal dispersion will generate vertical dispersion which will need additional correction. It is therefore preferable to place these quadrupoles in straight sections. Two families of skew quadrupoles in the utility straight sections and the IRs will be sufficient to control the effects due to the difference resonance $\nu_x - \nu_y = p$. These families will be placed so that the difference in phases $\psi_x - \psi_y$ differs by $\pi/2$ at the families. The coupling sum resonance $\nu_x + \nu_y = p$ may also need to be corrected (depending on the strength of the skew quadrupole errors). In this case an additional two families will be required, placed so that $\psi_x + \psi_y$ differs by $\pi/2$ at these families.

Chromaticity effects

The linear chromaticity is controlled by two families of sextupoles, one in each plane, placed in every arc cell. This will suffice provided the nonlinear change of tune with momentum is small over the required momentum aperture. If the global nonlinear chromaticity requires correction, then two families of sextupoles in each plane for the 90° cells will be required. It would therefore be desirable to place sextupoles (of say the F type) in every other cell on one bus and the other family of sextupoles in the other cells on another bus.

In addition to the chromaticity due to the quadrupoles, there is a contribution due to sextupole fields caused by iron saturation at fields close to 2 Tesla. This chromaticity must also be compensated by the chromaticity sextupoles. This has been discussed in the section on the dynamic aperture at collision.

If the beta function is strongly dependent on the momentum, then it can lead to an increased spot size if not corrected at the IPs and to emittance growth due to injection errors if not corrected at the injection point. Correcting the momentum dependence of the beta functions will require additional sextupole families.

For the IRs, a local chromaticity correction system was proposed for the SSC [37] which increased the momentum aperture from about $2.5\sigma_p$ with linear chromaticity correction to about $8\sigma_p$ with correction of the nonlinear chromaticity generated by the IRs. A similar such system may be required for the IRs if the momentum aperture needs to be increased.

Alignment tolerances in the IRs

These tolerances are more stringent for the IR quadrupoles than for any other magnets in the ring. Several criteria have to be met including:

- Dispersion at the IP should be small, both to attain maximum luminosity and to avoid synchro-betatron resonances.
- Beam excursions in the triplets should be limited to preserve the dynamic aperture.
- Separations between the beams at the parasitic collision points should not decrease.

In the IR quadrupoles the beta functions change rapidly and are not symmetric about the quadrupole center. As a consequence, pitch and yaw misalignments will introduce substantial beam separations at the IPs if not corrected. Due to the crossing angle a roll misalignment of an IR quadrupole will introduce orbit shifts in the plane orthogonal to the crossing plane. This is in addition to the extra coupling generated by the roll angle. Thus misalignments in all six degrees of freedom of these IR quadrupoles need to be well controlled and corrected.

Orbit offsets at the IPs

The orbit offset at the IP $z_{offset}(IP)$ due to a transverse displacement Δz_Q of an IR quadrupole (assumed to be at 90 degrees from the IP) is

$$\frac{z_{offset}(IP)}{\Delta z_Q} \propto \frac{\sqrt{\beta^* \beta_Q}}{F} \tag{3.6}$$

Here β_Q is the beta function at the quadrupole and F is the focal length of the displaced quadrupole. The maximum offset of the quadrupole that can be corrected with orbit correctors is proportional to this ratio $z_{offset}(IP)/\Delta z_Q$. In Table 3.5 we compare the parameters for the quadrupole where the beta function is the largest. Tolerances for the LHC quadrupoles were

Parameter	LHC IR	VLHC (LF) IR
β^* [m]	0.5	0.3
β^{max} [m]	4567	11263
Focal length F [m]	21.2	18.7
$z_{offset}(IP)/\Delta z_Q$	~ 2.3	~ 3.1

Table 3.5: Parameters of the strongest IR quadrupole in the LHC and the VLHC

derived in [34]. The rms tolerance for the offset was obtained to be 0.27 mm. Scaling this number by the ratio 2.3/3.1, we obtain a tolerance of 0.2 mm for the VLHC IR quadrupoles. This assumes that corrector strengths similar to those in the LHC (in kick angle) will be used in the VLHC.

Correctors to correct the orbit at the IP are best placed at 90 degrees from the IP. As in the LHC, correction packages with dipole and skew dipole correction coils should be placed at several high beta locations next to the IR quadrupoles. Spaces between Q2 and Q3 and after Q3 would be ideal locations for these correctors.

IR quadrupole roll angles

Tolerances on the allowed roll angles of the IR quadrupoles may be set by specifying the minimum tune split tolerable before correction. We will assume that this tune split due to roll angles in all sixteen quadrupoles from the two IRs is less than 0.05 before correction. An rms roll angle of 0.5 mrad can be tolerated for the IR quads, assuming that all the IR quadrupole assemblies include a skew quadrupole corrector.

Normally two families of skew quadrupoles are required to correct both the real and imaginary parts of the coupling resonance term. However the phase advance through the IRs is very small and so the imaginary part of the resonance term is negligibly small. Thus only a single skew quadrupole on each side of the IP will suffice to locally correct the coupling in the IR.

Table 3.6 summarizes the misalignment tolerances for the IR quadrupoles. These are based on scaling from tolerances derived for the LHC and should be replaced at a later stage with more exact calculations.

Misalignment	Tolerance
Offsets [mm]	0.2
Longitudinal placement [mm]	1
Roll [mrad]	0.5

Table 3.6: Misalignment tolerances for the VLHC IR quadrupoles derived by scaling from the LHC IR quadrupole tolerances [34].

Crossing angle

A crossing angle is required to separate the beams at the parasitic collisions. As is well known, the crossing angle has several effects on the linear and nonlinear optics and beam dynamics, including generation of dispersion due to orbit offsets in the quadrupoles, coupling due to skew multipole errors, and feed down of higher order multipoles. Local dispersion control is required to prevent dispersion waves from propagating into the arcs. This can be performed adjusting pairs of quadrupoles in the cells adjacent to the IRs where there is natural dispersion. A scheme such as this was proposed for the SSC [36]. Correction of local coupling from this and other sources will require skew quadrupoles in the IR as already mentioned. The linear effects from feed-down of higher order multipoles will be corrected by orbit and tune correctors. Nonlinear effects will require nonlinear correction packages in the IRs similar to those in the LHC and RHIC.

3.2.4 Ground motion and emittance growth

3.2.5 Collective effects

I have serious concern that the resistive wall consideration could lead to substantial rethinking of the bore tube design, and that material has not been reflected in the report as is.

For your urgent need of a one-page summary, my suggestion is then to integrate the latex file as is with the following contents:

A survey of the various instability and collective effects says that all these effects are OK except the transverse resistive wall instability.

To fight the transverse resistive wall instability, we have designed fancy feedback system. This FB system indeed is capable of suppressing the dipole multi-bunch resistive wall growth time of one turn. Exactly how fast is the growth rate is not 100% clear because theory of resistive wall impedance in this complicated environment (cold, thin coating, magnets outside, et cetera) is not easy to calculate. Whether it can suppress beyond one turn is yet to be demonstrated, although it looks promising.

Even if feedback can fight growth rates of less than one turn, the question still arises as to how to deal with the incoherent Laslett tune shifts caused by the resistive wall impedance. Both the coherent and the incoherent tune shifts can be as large as one unit, and they are not equal. During injection, the tune shifts as the beam current accumulates. How to control both the incoherent tune and the coherent tune so that they don't cross resonance lines is not clear. Perhaps a combination of time varying quadrupole strengths, and a one-turn feedback system would do the job? Are there cross-talk effects to worry about? Would such a combination of systems work in practice even if they work on paper?

In case we decide not to risk too much, there are ways to reduce the resistive wall effects. Some of them mentioned in the report. Problem is most of them will require rethinking of the present design, such as larger bore tube radius, etc. The point is that resistive wall considerations might affect the design in a big way.

3.3 STAGE 2: THE HIGH-FIELD RING

3.3.1 Luminosity versus energy

The High Field VLHC ring will be the first cryogenic collider to operate in the synchrotron radiation dominated regime, in which the radiation damping time is shorter than the storage time. In this regime there are practical and economic limits to the cryogenic system which can be installed. There is a maximum value P_{cryo} for the synchrotron radiation which can be absorbed in each ring. It is necessary to adjust the beam parameters to stay within the installed power limit, resulting in an average luminosity which depends on the beam energy E according to

$$L_{ave} \quad < \quad \frac{P_{cryo}}{E} \left(\frac{1}{N_{IP}\sigma_{tot}}\right)\left(\frac{T_0}{T_{store}}\right) \tag{3.7}$$

This is the exact form of the "maximum power law."

Although there is a clear advantage in reducing the storage time, T_{store} must remain significantly larger than T_{damp} in order to take advantage of radiatively damped beam sizes. Other factors (such as the refill time) will also play a role in determining the optimum value of T_{store}, but is safe to estimate that

$$\frac{T_0}{T_{store}} \quad \sim \quad 0.2 \tag{3.8}$$

Except for some uncertainty in this factor, the maximum power law clearly states that the installed capacity to absorb synchrotron radiation at cryogenic temperatures directly limits the attainable product of average luminosity and energy.

Similarly, if the beam stored energy per ring $U = NME$ must be kept below a maximum value – for example if the beam dump has a limited capacity – then

$$L_{ave} \quad < \quad \frac{U_{max}}{E} \left(\frac{1}{N_{IP}\sigma_{tot}}\right)\left(\frac{1}{T_{store}}\right) \tag{3.9}$$

Insofar as the stored energy is a practical limit to high field performance – to the product $L_{ave}E$ – then there is pressure to reduce T_{store}, and hence to increase the dipole field, to reduce the circumference, and to reduce the refill time.

Storage energy, E	87.5	TeV
Peak luminosity, L_{max}	2×10^{34}	$\mathrm{cm^{-2}s^{-1}}$
Collision debris power, per IP	73	kW
Dipole field at storage	9.765	T
Distance from IP to first magnet	30	m
Injection energy	10	TeV
Fill time	30	s
Acceleration time	2000	s
Synchrotron radiation damping time, T_0	2.48	h
Energy loss per turn, U_0	15.3	MeV
Natural transverse emittance (H)	0.0397	μm
Natural RMS momentum width	5.5	10^{-6}
Collision beta horz, β_x^*	3.7	m
Collision beta vert, β_y^*	0.37	m
Equilibrium emittance ratio, κ	0.1	
Initial bunch intensity, N	7.5	10^9
Beam current	57.4	mA
Synch. rad. power, per beam P	.88	MW
Dipole linear heat load	4.7	W/m
Stored energy, per beam U	3.9	GJ

Table 3.7: Nominal parameters for stores in the high field ring, using flat beams and doublet IR optics.

3.3.2 Operational performance

The High Field ring will be the first hadron collider able to join all electron colliders in taking advantage of naturally flat beams. The instantaneous luminosity is

$$L = \frac{M}{4\pi T} \frac{N^2\gamma}{\sqrt{\epsilon_x\epsilon_y\beta_x^*\beta_y^*}} \tag{3.10}$$

where T is the revolution period, and the flatness of the beam is conveniently measured by $\kappa = \epsilon_y/\epsilon_x$. The high field ring should be able to achieve $\kappa \ll 0.1$, in common with conventional electron storage rings.

The total number of protons in the ring, MN, is approximately set by the need to provide enough for "luminosity burn-off", plus an overhead fraction that is dumped at the end of the store. Since the number of bunches M is fixed, the need for a given peak luminosity then sets the single bunch population N. Nominal values for these and other parameters, including a conservative value of $\kappa = 0.1$, are given in Table 3.7.

It is the head on beam-beam interaction which sets the minimum horizontal emittance, whether the beams are flat or round. Figure 3.7 shows the horizontal and vertical emittances decreasing to plateau values of ϵ_x and ϵ_y that are consistent with the beam-beam limit, and which are maintained by transverse beam heating. Figure 3.8 shows the corresponding evolution of instantaneous luminosity, and its average, during the store.

The head on beam-beam interaction

The horizontal and vertical tune shift parameters for bi-gaussian round beams ($\beta_x^* = \beta_y^*, \epsilon_x^* = \epsilon_y^*$) are

$$\xi_x = \xi_y = \frac{r}{4\pi}\frac{N}{\epsilon_x} \tag{3.11}$$

By comparison, if the beams are very flat, $\kappa \ll 1$, then

$$\xi_x = \xi_y = \frac{r}{2\pi}\frac{N}{\epsilon_x} \tag{3.12}$$

The horizontal and vertical beam-beam parameters are made equal in the flat beam case by asserting that the β^* ratio is also κ

$$\kappa = \frac{\epsilon_y}{\epsilon_x} = \frac{\beta_y^*}{\beta_x^*} = \frac{\sigma_y^*}{\sigma_x^*} \tag{3.13}$$

Equations 3.11 and 3.12 show that, whether the beam is round or flat, the beam-beam parameter depends only on the horizontal emittance ϵ_x. Since the collision beta functions β_x^* and β_y^* do not influence the beam-beam parameters, they are adjusted (with a fixed ratio κ, and for given values of M, N, and ϵ_x) in order to achieve the required peak luminosity.

Then, re-writing Eqn. 3.10 as

$$L = \frac{M}{4\pi T} \frac{N^2\gamma}{\kappa\epsilon_x\beta_x^*} \tag{3.14}$$

it is explicitly clear that with flat beams the value of β_x^* can be increased by a factor of about $1/\kappa$, a large amount and a significant advantage. Equation 3.13 then shows that the value of β_y^* is about the same for flat or round beams.

Crossing angles and parasitic beam-beam collisions.

The horizontal and vertical tune shifts due to a single parasitic collisions are

$$\Delta q_{x,y} \approx \pm\frac{rN}{2\pi\gamma}\frac{\beta_{x,y}}{\Delta^2} \tag{3.15}$$

where the approximation is valid if the full beam separation Δ is much greater than both horizontal and vertical beam sizes, so that the beam acts like a moving line charge.

If the beams are thoroughly separated (into separate beam pipes, or with very large separations) at a distance L_{sep} from the IP, then there are $4\ L_{sep}/S_B$ parasitic collisions around each IP, where S_B is the longitudinal bunch separation. The total tune shifts from all parasitic collisions in one interaction region are

$$\Delta Q_{x,y} \approx \pm\frac{rN}{2\pi\gamma}\frac{4}{S_B}\frac{L_{sep}}{\beta_{x,y}^*\alpha^2} \tag{3.16}$$

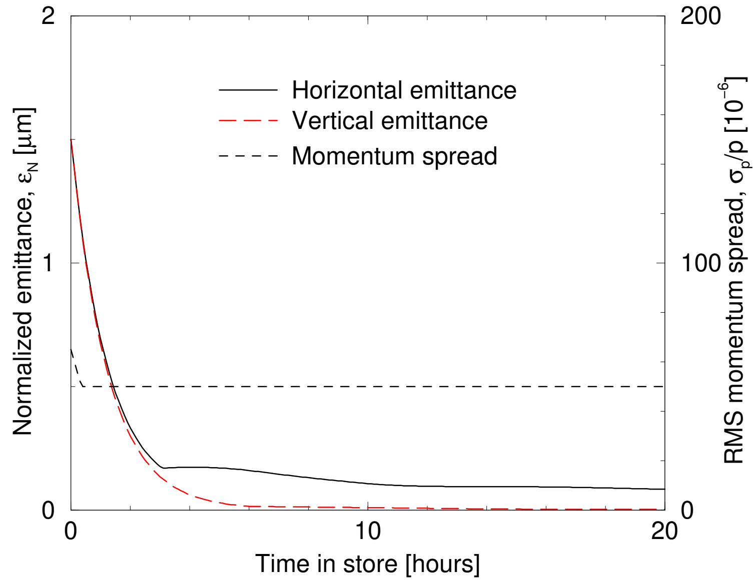

Figure 3.7: Evolution of the transverse emittances and the rms momentum spread during a store.

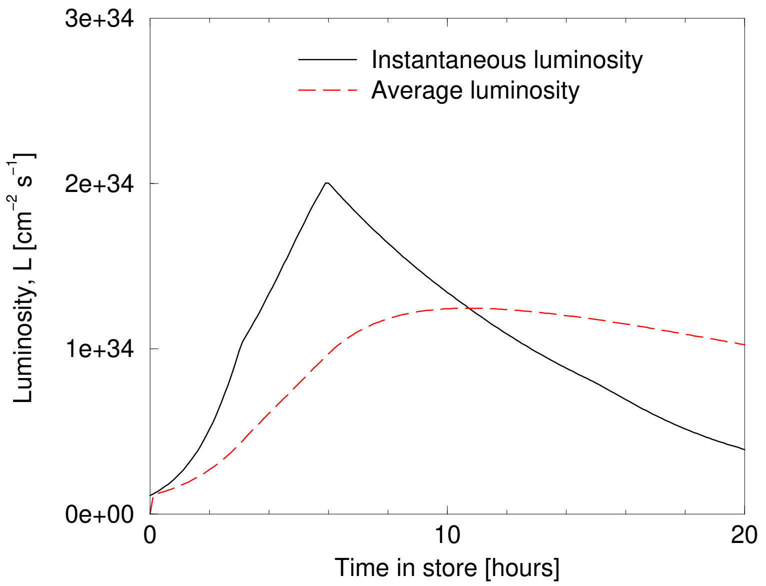

Figure 3.8: Evolution of the instantaneous and average luminosities, during a store.

where the approximation is most valid if the beams are fuly separated before the first IR quadrupole.

The horizontal beta function at each collision is much less than the vertical

$$\frac{\beta_x}{\beta_y} \approx \frac{\beta_y^*}{\beta_x^*} = \kappa \tag{3.17}$$

so that, taking Eqns 3.16 and 3.17 together gives

$$\Delta Q_x \quad \simeq \quad -\kappa\,\Delta Q_y \tag{3.18}$$

The horizontal tune shift is greatly supressed with flat beams, to be much smaller than it is with round beams – if the values of L_{sep} and α compare favorably between the two cases.

3.3.3 Advantages and disadvantages of flat beams

All electron colliders, whether circular or straight, take advantage of flat beams and use doublet optics. However, it has never before been possible to use flat beams in a hadron collider. Flat beams have the advantages and disadvantages discussed below, which continue to be investigated. Flat beams require the first quadrupole on both sides of the IP to be vertically focusing to both counter-rotating beams (whether the crossing angle is vertical or horizontal). Thus, the optics must be symmetric across the IP, and the first quadrupole must be a 2-in-1 magnet.

Table 3.8 compares the performance of flat and round beam in the high field ring. In both cases the beam-beam limit of ξ = .008 is reached 5 or 6 hours into the store, when the luminosity is at its peak. The horizontal and vertical emittances values recorded in Table 3.8 are those which are initially maintained (preventing further emittance shrinkage) when the horizontal and vertical beam-beam parameters first saturate. The same peak luminosity is achieved in both flat and round beam cases by adjusting the horizontal and vertical β^* values.

	FLAT	ROUND
Flatness parameter, κ	0.1	1
Beam-beam parameter $\xi_x = \xi_y$	.008	.008
Peak luminosity L (10^{34} cm^{-2}s^{-1})	2.0	2.0
Initial bunch intensity N (10^9)	7.5	7.5
Collision beta horz β_x^* (m)	3.7	0.71
Collision beta vert β_y^* (m)	0.37	0.71
Maximum beta horz $\widehat{\beta_x}$ (km)	7.84	14.58
Maximum beta vert $\widehat{\beta_y}$ (km)	10.75	14.58
Horizontal emittance ϵ_x (μm)	.161	.082
Vertical emittance ϵ_y (μm)	.016	.082
Collision beam size horz σ_x^* (μm)	2.53	0.79
Collision beam size vert σ_y^* (μm)	0.25	0.79
Maximum beam size horz $\widehat{\sigma}_x$ (μm)	116	113
Maximum beam size vert $\widehat{\sigma}_y$ (μm)	43	113
Total crossing angle α (μr)	10.0	10.0
Separation distance, L_{sep} (m)	30	120
Number of long range collisions per IR	20	84
Long range tune shift per IR, horz $\lvert\Delta Q_x\rvert$	.0008	.0166
Long range tune shift per IR, vert $\lvert\Delta Q_y\rvert$	.0081	.0166

Table 3.8: Flat and round beam performance parameters, quoted after about 6 hours at the “early plateau” just after peak luminosity, when the horizontal and vertical beam-beam parameters are both saturated.

A major advantage of flat beams comes from the order of magnitude increase of β_x^*, by a factor of about $1/2\kappa$. Slightly offsetting this advantage, the vertical β_y^* decreases by a factor of about 2. Early separation pushes the first quadrupole further from the IP, but the values of $\widehat{\beta}$ recorded in Table 3.8 still show the strong advantage of doublet optics.

Table 3.8 shows a factor of two reduction in the vertical, and an order of magnitude reduction of approximately $2/\kappa$ in the horizontal. The value of the total crossing angle α is set to be identical with flat or round beams – and is independent of the plane of the crossing angle. There are far fewer parasitic collisions per interaction region with flat beams, than with round beams.

The most significant disadvantage is that the design of the first quadrupole is difficult. A 2-in-1 magnet with relatively close separation will not have as good field quality a single bore element. Nonetheless, the maximum beta $\widehat{\beta}$ is significantly less in the doublet design, so the tolerable field errors are larger. The preliminary reference harmonics are the subject of on-going Accelerator Physics and Magnet Physics evaluations.

Another difficulty is that neutral particles generated at the IP will aim head-on for the center of the first 2-in-1 quadrupole. Each IR has $\sim$36 kW of beam garbage going off in each direction, and the neutrals carry about 30% (11 kW) of this power. The severity of this problem is difficult to quantify without a full blown energy deposition simulation of the beam losses, and a detailed draft design of the first quadrupole. Although these energy deposition simulations have begun, it is clear that here, too, a more detailed analysis is required.

A lack of energy flexibility may be a disadvantage to flat beams. The radiation damping time scales like $1/E^3$, so if the collision energy is halved from 87.5 TeV to 43.75 TeV, then the time increases to about 20 hours, and flat beams are no longer viable. If such a large dynamic range of collision energies is desired (at fixed geometry) then one possibility is to arrange the IR quadrupoloes so that both doublet and triplet optics are possible. A lattice has been demonstrated in which 4 IR quadrupoles can swing either way – can act as a doublet or as a triplet [9].

An operational disadvantage is the need for careful tuning to keep the vertical emittance small. Electron rings routinely acheive beam flatnesses in the range $0.001 < \kappa < 0.01$ by controlling 2 linear quantities: the vertical dispersion in the arcs, and global betatron coupling. The mathematics behind the control room algorithms for such clean living is well understood, and shows no sign of significant differences between the electon and hadron colliders, except for the much different radiation damping times. It is not unreasonable for high field ring studies to also consider less conservative flatness values, of say $\kappa \approx 0.01$, which are closer to every day electron storage ring experience.

3.3.4 Lattice

The lattice geometrically matches the low field (LF) ring lattice so that they both fit in the same tunnel. See Table 3.9 for a selection of HF lattice parameters. The arcs are composed of FODO cells of separated function magnets. The dispersion suppressors are also conventional FODO designs.

Horizontal tune	218.19	
Vertical tune	212.18	
Transition gamma	194.13	
Maximum arc beta	459	m
Maximum arc dispersion	1.42	m
Vertical β^* (store)	0.37	m
Horizontal β^* (store)	3.7	m
Maximum $\widehat{\beta}$, injection	.61	km
Maximum Horz $\widehat{\beta}$, store	7.84	km
Maximum Vert $\widehat{\beta}$, store	10.75	km

Table 3.9: Short list of some high field lattice parameters.

Doublet IR optics approach

The IR gives 30 m free space from the interaction point to the first magnetic element. For the doublet optics, the first magnet encountered is a high field small bore magnet of 16 T field. This can handle the beams until they total separation becomes

8 mm. Then the beams enter a lower field, 12 T, magnet with a larger bore. These beam separation dipoles bend the beam vertically. This crossing region requires that the beam separation at the first quadrupole be 30 mm. With these dimensions the first quadrupole is limited to 400 T/m gradient. As the beams separate, a higher quadrupole field can be attained with a limit of 600 T/m.

With this design of the crossing region, an IR is designed to fit at two location in the on-site utility region. The β^* can be varied from 0.37 m to 7.12 m (vertically, β^* horizontally is 10 times larger). The maximum beta $\widehat{\beta}$ is 10.6 km with the collision optics and only about 760 m at injection. Figure 3.9 shows the collision optics of the interaction region.

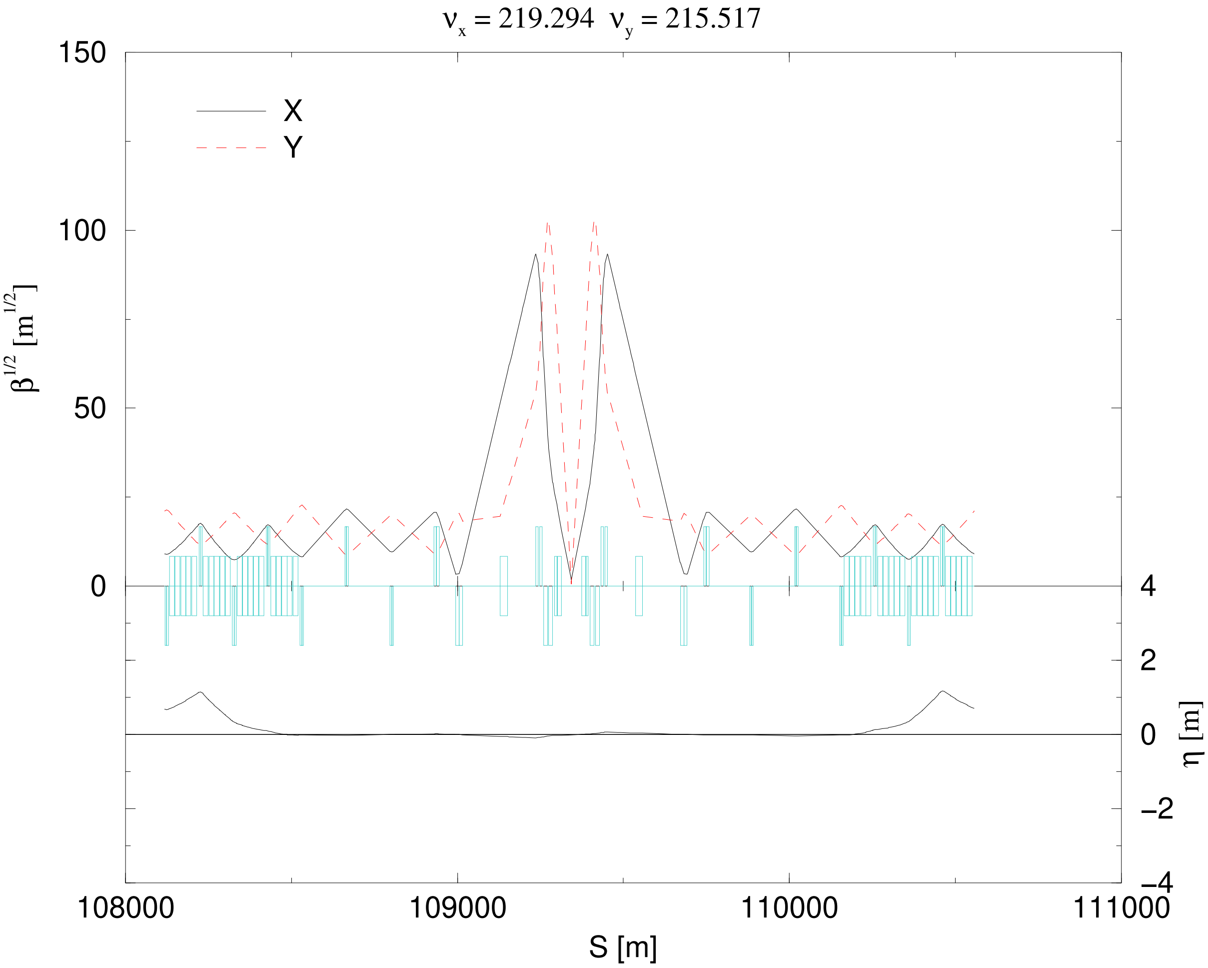

Figure 3.9: Lattice functions near the IP in collision optics, using doublet focusing.

Triplet IR optics approach

Although doublet optics are more naturally suited to the flat beams of the high-field ring, collisions could be created instead using anti-symmetric triplets for the final focusing. The "round beam" model discussed here is qualitatively similar to the low-field IR design. The triplet quadrupoles are 400 T/m single-bore magnets. Four additional circuits, comprising double-bore 400 T/m magnets are also used for optical matching. With a total of 6 independently-tunable quadrupole circuits available it is possible to match the four β's and α's from the IP into the regular FODO cells, plus hold the phase advance $\Delta\mu$ constant across the IR through the squeeze from $\beta = 12.0 \rightarrow 0.50$ m. Fixing $\Delta\mu$ eliminates the need for a special phase trombone somewhere in the ring to maintain the nominal operating point. Figure 3.10 shows the lattice functions through the insertion region at collision.

The circulating beams are separated vertically everywhere in the ring, except in the triplet quadrupoles. Four 10 T dipoles between the Q3 and Q4 quadrupoles bring the beams together at the entrance to the triplet for collisions at the IP. Dipoles

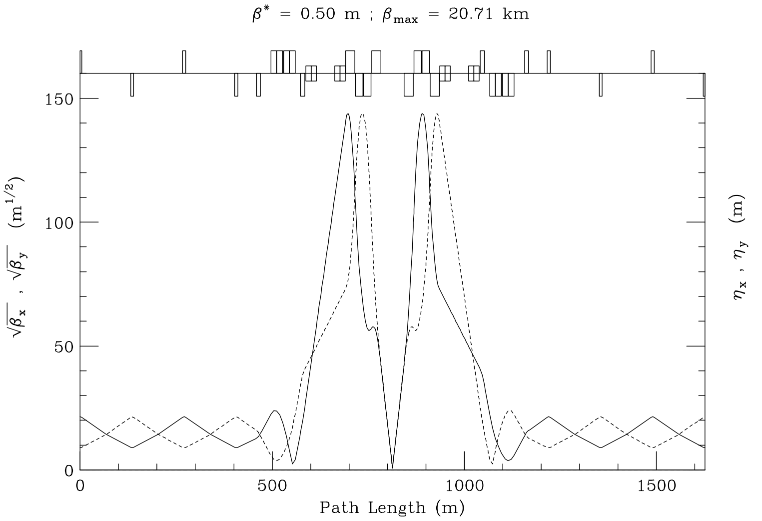

Figure 3.10: Lattice functions near the IP in collision optics, using triplet focusing.

downstream of the IP separate the beams again vertically and channel them back into the upper and lower rings. A half-crossing angle of 28.8 μr gives 10σ separation between the beams at the first parasitic crossing 2.823 m downstream of the IP (ϵ_N = 1.5 μm at 87.5 TeV/c).

3.3.5 Magnet aperture and field quality

The effect of the magnetic field quality on the dynamic aperture was investigated at the injection energy of 10 TeV. At injection the beam size has its maximum and errors in the arc magnets dominate the dynamic aperture. With the current one-turn injection scenario, a storage time on the order of seconds is sufficient. To estimate the effect of the magnetic field errors on the single particle dynamic, the nonlinear chromaticity, the tune spread from nonlinear fields and the 1000-turn dynamic aperture were computed. 1000 turns is equivalent to 0.7 seconds real time in the VLHC. Experiments have shown that the dynamic aperture can be computed for storage rings with nonlinear field errors within a 30% error when the field errors are well known [13, 14]. For a future machine, however, a larger safety margin is required.

In the lattice that is used for the evaluation, no interaction regions were inserted since the dynamic aperture is dominated by the arcs. Arc magnet errors at injection were estimated for a 2.0 T field in the dipoles. The systematic errors were computed as the maximum possible absolute value with given mean and uncertainties. Random errors were created from a Gaussian distribution, cut at two sigma.

Quadrupoles were horizontally and vertically displaced randomly with a Gaussian distribution with a 0.3 mm rms value, cut at three sigma. In addition, beam position monitors were displaced with a 0.2 mm rms value. The resulting non-zero closed orbit was corrected to zero in the beam position monitors with horizontal orbit correctors at focusing quadrupoles and vertical orbit correctors at defocusing quadrupoles. Skew quadrupole errors in the arcs were disregarded and no coupling correction was necessary. The transverse tunes were set to (218.190,212.180). Both horizontal and vertical chromaticity were set to 2.

No synchrotron motion was included but particles had a relative momentum deviation of $\Delta p/p = 7.2 \cdot 10^{-4}$, corresponding to three times the rms of the momentum distribution. The physical aperture of 1 cm in the arcs corresponds to 35 σ of the transverse beam size in the quadrupoles. Fig. 3.11 shows dynamic aperture averaged over 10 seeds along with the minimum of the 10 seeds. The error bars of the average dynamic aperture are the rms value of 10 seeds.

Although linear coupling and synchrotron motion were disregarded in the determination of the dynamic aperture, the field quality with the magnet field errors used is sufficient for injection.

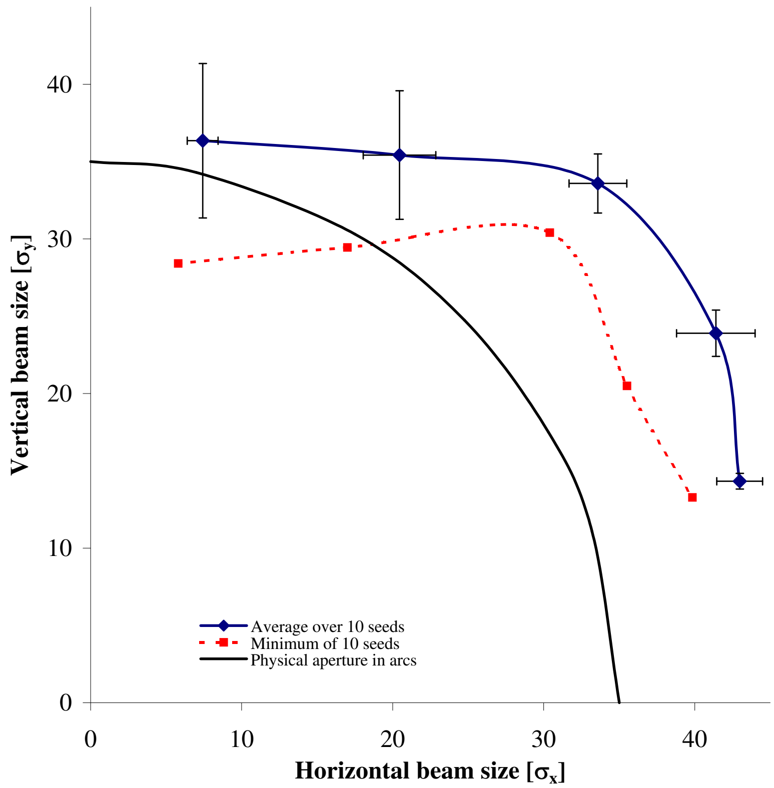

Figure 3.11: 1000-turn dynamic aperture. Shown are the average over 10 seed, the minimum of 10 seeds and the physical aperture, in in units of the transverse rms beam size. The error bars of the average dynamic aperture are the rms value of 10 seeds.

3.3.6 Tolerances and Corrections

In this section we consider the effect of magnet misalignments as well as the effect of main dipole and quadrupole field errors on the beam orbit and betatron tunes. We discuss the tolerances for misalignment and field errors listed in Table 3.10. To this purpose we use the high-field storage optics with $\beta_x^* = 3.7$m and $\beta_y^* = 0.37$m.

Orbit errors

Possible sources of orbit error include transverse quadrupole misalignments (in both the horizontal and vertical directions), main dipole field integral errors (for the horizontal orbit), and roll of the main dipole magnets (for the vertical orbit). In order to estimate and compare the value of the orbit distortion coming from these different types of error sources, the rms closed orbit has been calculated. The calculations assumed the rms magnet misalignments listed in Table 3.10. Each of five different individual perturbation sources were considered in turn. In some cases the errors are introduced in all magnets in the accelerator arcs, while in others the errors are applied to the quadrupoles of one of the interaction region doublets. In the interaction region doublets there is one corrector per plane. The biggest effect comes from quadrupole offsets. The dipole integral field error and dipole roll errors quoted in Table 3.10 have little influence on the required corrector strength.

Tune error, coupling and IR chromatic effects

The betatron tune shift caused by an rms quadrupole field error of 10^{-4} and the betatron coupling effect produced by rms quadrupole rolls of 1 mrad have been calculated. The tolerance for arc quadrupole error can be put at 5×10^{-4} providing a 2.5 rms beta-beating value of about 9% is acceptable. A small number of quadrupole correctors placed in the arcs will easily compensate for this beta-beating. Field errors in interaction region quadrupoles can be corrected by adjusting the currents of power supply for these quads. After the current adjustment is done the current fluctuations should be kept well below the 10^{-4}

RMS ERROR	ARC	IR	
QUADRUPOLES			
Transverse offset	0.25	0.2	mm
BPM to quad offset	0.15	0.1	mm
Roll	0.5	0.5	mrad
Field Error $\Delta K/K$	0.5	0.1	10^{-3}
DIPOLES			
Roll	0.5	0.5	mrad
Field Error $\Delta B/B$	0.5	0.5	10^{-3}

Table 3.10: Tolerance summary for magnet alignment

level. Both global correction in the arcs and local skew quadrupole correction in the interaction regions are required for the compensation of betatron coupling effects. With these correection systems in place it is possible to relax the quad roll tolerances to about 0.5 mrad.

Because of the very large maximum β values in the interaction region quadrupoles, the chromatic effects produced by these quadrupoles have been evaluated. For the design value of rms momentum spread of 5×10^{-5} the amplitude of the chromatic vertical beta-wave was found to be just a few percent. Thus the effect is not large, mainly due to the small rms momentum spread. The vertical chromaticity produced by the quadrupoles from one interaction region has been found to be about -42. The horizontal chromatic effects are smaller than the vertical.

Corrector strengths

The maximum dipole corrector strengths displayed in Table 3.11 are 2.5 times the rms value when all error sources are combined in quadrature. Assuming a maximum achievable field of 3.5 T for the IR dipole correctors, and 2.2 T for the arc dipole correctors, magnetic lengths of 1.05 m in the arcs and 2.5 m in the IRs are required. If the maximum corrector strengths are increased to higher values than those cited in Table 3.11, then the corresponding tolerances in Table 3.10 can be relaxed accordingly.

Even the maximum dipole corrector strengths listed in Table 3.11 cannot make up for the magnet alignment diffusion caused by ground motion. Ground motion might put magnet offsets well beyond the defined tolerances after a few years of movement. Thus, periodic magnet realignment will be necessary. Some means to simplify the realignment procedure, such as using stepping motors, should be evaluated.

ARC CORRECTORS		
Dipole magnetic length	1.05	m
Dipole max strength	2.3	Tm
Skew quad length	0.95	m
Skew quad max strength	95	T
Sextupole magnetic length	0.95	m
Sextupole max strength, $L(d^2B/dx^2)$	7400	T/m
IR CORRECTORS		
Magnetic length	2.5	m
Dipole max strength	8.6	Tm
Skew quad max strength	95	T

Table 3.11: Corrector magnetic lengths and strengths. The maximum strengths are 2.5 times the rms value required when all contributions are added in quadrature.

3.3.7 Collective effects

3.4 SUMMARY

```
LF
--

Instabilities.  One turn feedback.

Lower beta^* & N??



HF
--

We can do better if we make masks work (HF).

eg power density.

Discuss limits (eg cryo power, IR debris power 37 kW/beam).  Learn how
to go to 50 ?  What are the omplisactions?

Luminosity leveling - dynamic beta^* ....

Discussion of Chapter 1 table (L vs E).
```

Bibliography

[1] P. Limon (editor), *VLHC Feasibility Study*, FNAL ??, May 2001.

[2] J.P. Koutchouk, *The LHC Dynamic Aperture*, PAC 1999.

[3] V. Shiltsev, *Proc. ICFA Workshop on Ground Motion*, Nov. 2000, SLAC; http://www-project.slac.stanford.edu/ls/wkshp/GM2000

[4] V. Shiltsev, FNAL TM-1987, 1996.

[5] B. Baklakov et al, PRST Accel. Beams, 031001, 1998.

[6] A. Burov et al, *Beam Stability Issues in a Very Large Hadron Collider*, p. 194 NIMA 450, 2000.

[7] J. Wei, *Intra-beam scattering scaling for Very Large Hadron Colliders*, BNL C-A/AP/38, Feb. 2001.

[8] S. Peggs, F. Dell, *Tolerable systematic errors in Really Large Hadron Colliders*, Snowmass, 1996.

[9] S. Peggs, M. Harrison, F. Pilat, M. Syphers, *Flat beams in a 50 TeV hadron collider*, Vancouver PAC 97, 1997.

[10] S. Peggs et al, *Lattices for a high-field 30 TeV hadron collider*, Snowmass, 1996.

[11] J. Wei, S. Peggs, *Interaction region analysis for a high-field hadron collider*, Snowmass, 1996.

[12] S. Peggs et al, *Lattice optimization for a Really Large Hadron Collider*, Barcelona EPAC 96, 1996.

[13] W. Fischer, *An Experimental Study on the Long-term Stability of Particle Motion in Hadron Storage Rings*, PhD thesis Hamburg University, DESY 95-235 (1995) and CERN SL/96-10 (AP), 1996.

[14] W. Fischer, M. Giovannozzi and F. Schmidt, *Dynamic Aperture Experiment at a Synchrotron*, Phys. Rev. E, Vol. 55, Number 3, p. 3507, 1997.

[15] Stimulated desorption experiments??

[16] Stimulated desorption experiments??

[17] Condon & Odishaw, *Handbook of Physics*, pg 4-72, 1967.

[18] Gary McIntyre, private communication.

[19] J.M. Wang, SLAC summer school, 1985.

[20] J. Marriner, FNAL tech note, September, 1997.

[21] M. Blaskiewicz, W.T. Weng, Phys. Rev. E, Vol 50, # 5, p 4030, 1994.

[22] Y.H. Chin, CERN/LEP-TH/88-05, 1988.

[23] A. Chao, *Physics of Collective Beam Instabilities in High Energy Accelerators*, John Wiley and Sons, 1993, and references therein.

[24] S. Peck, *Minimizing Chromaticity in Interaction Regions with Long Weak Quadrupoles* Snowmass 1984, p. 384.

[25] E. Keil, R. Talman, ...

[26] T. Sjoestrand, *PYTHIA 5.7 and JETSET 7.4, Physics and Manual*, Computer Physics Commun. 82 (1994) 74.

[27] L. Vos, LHC Project Note 150, CERN, 1998.

[28] S.Y. Zhang, C-AD AP Tech. Note, in preparation, 2001.

[29] O. Gröbner, LHC Project Report 127, 1997.

[30] H. Seiler, J. Appl. Phys. 54, R1, 1983.

[31] David Neuffer, Particle Accelerators **23** (1988), 21.

[32] F. Ostiguy, *personal communication*, March 19, 2001

[33] P. Schlabach, *Cancellation of the harmonics of the two cold masses in a Q2*, TD Note (2000)

[34] T. Sen, *Alignment tolerances of IR quadrupoles in the LHC*, FNAL-Conf-99-304 (October 1999)

[35] G. Ambrosio, *personal communication*, March 22, 2001

[36] Y. Nosochkov and D. Ritson, *Provision of IP crossing angles for the SSC*, SSCL-Preprint-367 (1993)

[37] T. Sen et al, *Chromaticity Correction for the SSC Collider Rings*, Proc. 1993 IEEE Part. Acc. Conf, 143 (1993)

[38] W. Foster, *Staged VLHC Parameter List Version 0.4 2/23/01*, private communication.

[39] See for example, K.Y. Ng, *Impedances and Collective instabilities of the Tevatron at Run II*, Fermilab Report TM-2055, 1998.

[40] M. Blaskiewicz, *Stability issues for the high field VLHC*, VLHC Instability Workshop, SLAC March 21-23, 2001, Proc. at http://www.slac.stanford.edu/∼achao/VLHCworkshop.html.

[41] D. P. Barber and A. De Roerk (editors), DESY-PROC-1999-03, (1999)

[42] V. A. Anferov, *Phys.Rev.Lett.* **83** 14, p.2738–2740, (1999)

[43] S. R. Mane, *Phys.Rev. A* **36** (1) p.105–130, (1986)

[44] M. Vogt, PhD–thesis, University of Haburg, FRG, (2000) also: DESY-THESIS-2000-054, (2000) and `http://www-mpy.desy.de/proton_pol/hoffpaper/00vogt.ps.gz`

[45] Ya. S. Derbenev and A. M. Kondratenko, *Sov.Phy. JETP* **35** (2) pp.230, (1972) and *Sov.Phy. JETP* **37** (6) pp.968, (1973)

[46] D. P. Barber, K. Heinemann and G. Ripken, DESY-M-92-04 (1992), 2-nd revised version (1999)

[47] K. Yokoya, DESY-86-57, (1986)

[48] G. H. Hoffstaetter, Habilitation–thesis, Technical University Darmstadt, FRG, (2000), (to be published by Springer Verlag)

[49] D. P. Barber, K. Heinemann, G. H. Hoffstaetter and M. Vogt, DESY-HERA-96-07 (1996)

[50] G. H. Hoffstaetter and M. Vogt, The `SPRINT` Manual, to be published in 2001

[51] J. A. Johnstone, private communication (2001)

[52] S. Y. Lee, Spin Dynamics and Snakes in Synchrotrons, World Scientific, (1997)

[53] K. Yokoya, DESY-99-006, (1999)